ACS central science

http://pubs.acs.org/journal/acscii

Research Article

# Optical Control of Phosphatidic Acid Signaling

Reika Tei,[#] Johannes Morstein,[#] Andrej Shemet, Dirk Trauner,[*] and Jeremy M. Baskin[*]

Cite This: *ACS Cent. Sci.* 2021, 7, 1205−1215

Read Online

ACCESS | Metrics & More | Article Recommendations | Supporting Information

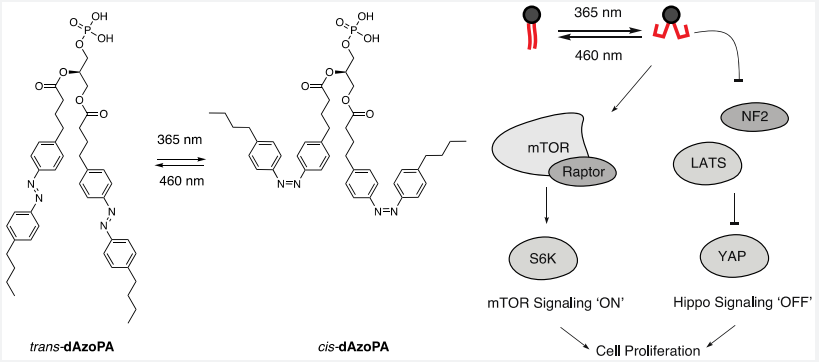


**ABSTRACT:** Phosphatidic acids (PAs) are glycerophospholipids that regulate key cell signaling pathways governing cell growth and proliferation, including the mTOR and Hippo pathways. Their acyl chains vary in tail length and degree of saturation, leading to marked differences in the signaling functions of different PA species. For example, in mTOR signaling, saturated forms of PA are inhibitory, whereas unsaturated forms are activating. To enable rapid control over PA signaling, we describe here the development of photoswitchable analogues of PA, termed **AzoPA** and **dAzoPA**, that contain azobenzene groups in one or both lipid tails, respectively. These photolipids enable optical control of their tail structure and can be reversibly switched between a straight *trans* form and a relatively bent *cis* form. We found that *cis*-**dAzoPA** selectively activates mTOR signaling, mimicking the bioactivity of unsaturated forms of PA. Further, in the context of Hippo signaling, whose growth-suppressing activity is blocked by PA, we found that the *cis* forms of both **AzoPA** and **dAzoPA** selectively inhibit this pathway. Collectively, these photoswitchable PA analogues enable optical control of mTOR and Hippo signaling, and we envision future applications of these probes to dissect the pleiotropic effects of physiological and pathological PA signaling.

## INTRODUCTION

Phosphatidic acids (PA) are a class of signaling lipids that mediate diverse and distinct physiological processes in mammalian cells.[1−3] Production of PA is elevated in many cancers, likely due to its pleiotropic effects in promoting cell proliferation.[4,5] In particular, PA regulates two major pathways that control cell growth and organ size, mammalian target of rapamycin (mTOR) and Hippo signaling.[6−8] mTOR signaling is a central pathway that regulates cell growth, and its activation enhances cell proliferation by promoting biosynthesis and suppressing autophagy.[9] By contrast, activation of Hippo signaling restrains organ size by inhibiting cell proliferation and stimulating apoptosis.[10] Notably, the reported activities of PA include both activation of mTOR and inhibition of Hippo signaling, thus resulting in progrowth effects in both pathways, yet via independent mechanisms.[8] However, it is unclear if, in all contexts, these pathways are directly regulated by PA or if they involve indirect mechanisms that are dependent on PA being metabolized to other lipids.[11,12]

PAs form a central hub in glycerophospholipid metabolism and are potent signaling agents. Their biosynthesis occurs via at least three major routes and on multiple organelle membranes, and they can be rapidly interconverted with other lipids.[13] Further, though all PAs contain a signature phosphate monoester headgroup, the acyl tail composition can vary, and not all PA species have equivalent bioactivities. This dynamic metabolic network and structural diversity complicate efforts to understand how individual PA species control specific signaling outcomes.

Frontier approaches that allow for high spatiotemporal and molecular control could therefore facilitate the study of PA physiology. Our laboratory has recently developed an optogenetic approach that features controlled PA synthesis

**Received:** April 9, 2021
**Published:** July 14, 2021

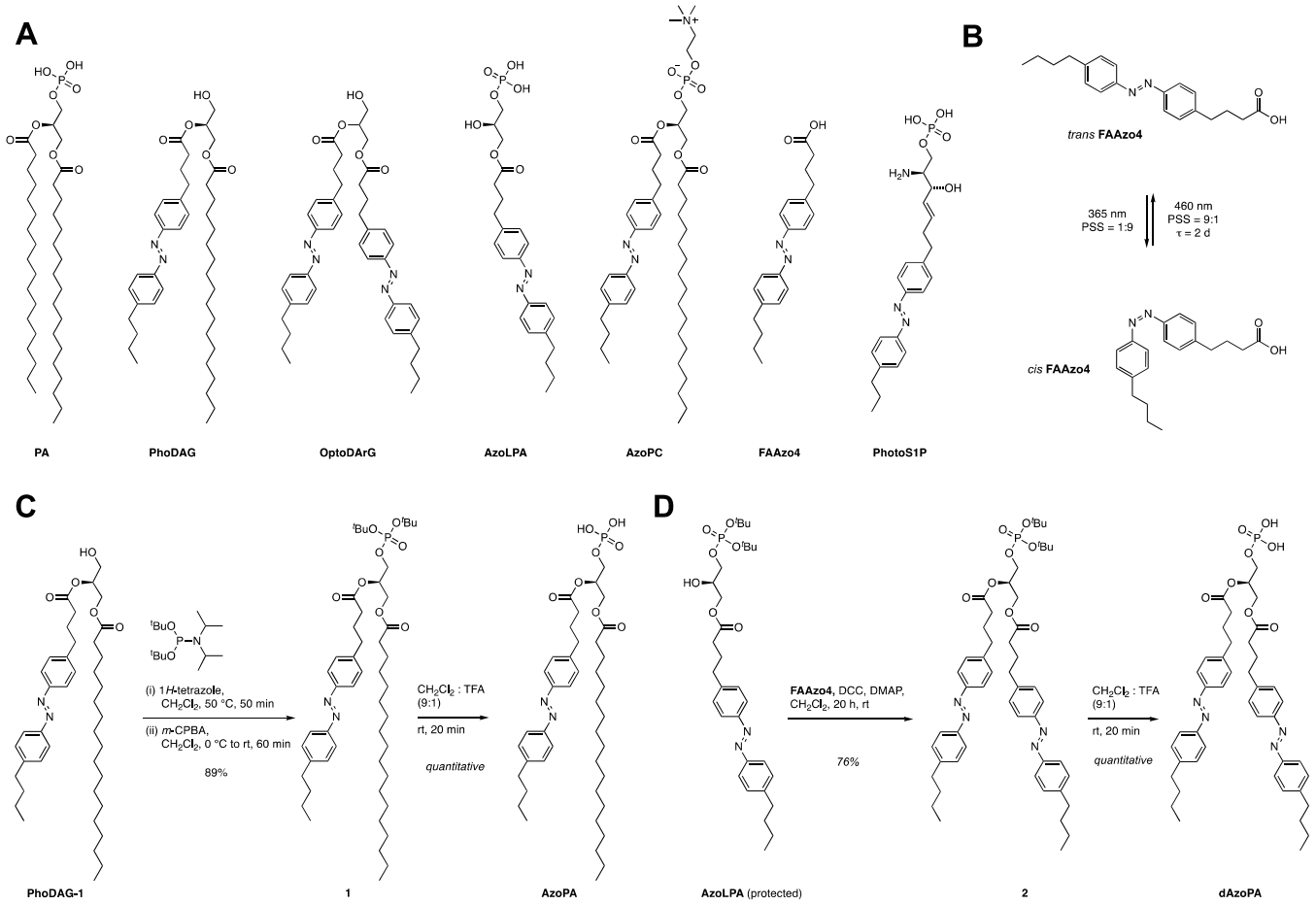


**Figure 1.** Design and synthesis of the photoswitchable PA variants **AzoPA** and **dAzoPA.** (A) Chemical structures of PA and previously developed photoswitchable lipids, including **PhoDAG**, **OptoDArG**, **AzoLPA**, **AzoPC**, **FAAzo4**, and **PhotoS1P**. (B) Photoisomerization of an azobenzene-containing photolipid (shown: **FAAzo4**). (C) Synthesis of **AzoPA** from **PhoDAG-1**. (D) Synthesis of **dAzoPA** from a protected form of **AzoLPA**.

by engineered phospholipase Ds at organelle-level resolution and with the temporal precision of light.[14] This approach, which enables the dissection of PA functions at different cellular locations, revealed that PA pools specifically generated at the plasma membrane attenuate Hippo signaling. Yet, optogenetics tools relying on a phospholipase D have limited control over PA acyl tail composition and rely on genetic manipulations, potentially restricting the scope of *in vivo* applications.

A photopharmacological strategy[15−17] to optically control PA signaling could potentially complement this approach and even offer certain advantages. Such tools would retain the exquisite spatiotemporal control afforded by light activation. Additionally, because exogenously added photopharmacological agents would not rely on endogenous metabolism, they would afford complete control over the molecular composition of the target lipid species. Photolipids would also not require genetic perturbations and could thus be used in a broader set of biological systems.

Photocaged lipids have emerged as attractive strategy for the photoactivation of lipids through cleavage of a photosensitive protection group to reveal the native lipid.[18] Photocaged versions of phosphatidic acid[19,20] have been used to control the activation of matrix metalloproteinase 2[21] and flagellar excision.[22] Chemical modifications of the photosensitive groups also allow for subcellular targeting.[23−26]

As an alternative strategy to precisely control lipid functions in a cellular context, we have begun to systematically explore photoswitchable lipids. These lipid analogues exhibit a hydrophobic azobenzene photoswitch in their lipid tail, allowing for retention of the headgroup and biological function of lipids while often enabling optical control of that function through differences in the bioactivities of the *trans* and *cis* forms.[27] Photoswitchable lipids have yielded optical control of several biological targets, including ion channels,[28−30] G-protein-coupled receptors (GPCRs),[31−33] enzymes,[34,35] nuclear hormone receptors,[36−38] immune receptors,[39,40] as well as membrane properties.[41−46] Among the photolipids developed to date several are analogues of lipids implicated in PA metabolism, which include fatty acids (**FAAzo4**),[28] diacylglycerol (**PhoDAG** and **OptoDArG**),[29,34] lysophosphatidic acid (**AzoLPA**),[33] and phosphatidylcholine (**AzoPC**)[44] (Figure 1A,B).

Yet, a major omission in the growing compendium of photoswitchable lipids are analogues of PA itself, which we reasoned would represent powerful tools to manipulate and understand PA signaling. Herein, we report the development of photoswitchable analogues of PA and demonstrate that they are versatile tools for the optical control of PA-dependent signaling in both the mTOR and the Hippo pathways. Interestingly, though the *cis* forms of the two photoswitchable PA analogues are more active than their corresponding *trans* forms, we found differences in abilities of these probes to


https://doi.org/10.1021/acscentsci.1c00444
ACS Cent. Sci. 2021, 7, 1205−1215

regulate the mTOR and Hippo pathways. These results provide a roadmap for using these photolipids to control selective outputs of PA signaling, suggesting their use to dissect the pleiotropic effects of this lipid signaling agent.

## RESULTS

**Design, Synthesis, and Photophysical Characterization of Photoswitchable PA Analogues.** The two acyl chains of phosphatidic acid can exist in saturated or unsaturated forms. Notably, the signaling function of PA is strongly altered by lipid saturation. In mTOR signaling, PA with two saturated acyl chains (16:0/16:0) inhibits mTOR signaling,[47,48] whereas forms of PA with monounsaturated acyl chains in one or two positions stimulate mTOR signaling. Thus, we envisioned the development of photoswitchable analogues of PA in which the azobenzene N=N double bond is near the middle of the lipid tail, which corresponds to the C=C *cis* double bond in unsaturated forms of PA. In previous work, we and others have found that *cis* forms of azobenzene-containing lipids exhibit bioactivities corresponding to mono- and/or polyunsaturated lipids.[28,29,33,34]

Two photoswitchable analogues of PA were prepared: **AzoPA**, which bears **FAAzo4** at the sn-2 position and stearic acid at the sn-1 position, and **dAzoPA**, which contains **FAAzo4** at both positions. The synthesis of **AzoPA** began from the previously published photoswitchable analogue of diacylglycerol, termed **PhoDAG-1**[34] (Figure 1C). Phosphorylation of **PhoDAG-1** with di-*tert*-butyl-*N*,*N*-diisopropyl phosphoramidite and subsequent oxidation yielded compound **1**. **AzoPA** was obtained through deprotection of **1** with TFA. The synthesis of **dAzoPA** was achieved starting from di-*tert*-butyl-protected **AzoLPA**[33] through acylation with **FAAzo4** and subsequent deprotection with TFA (Figure 1D).

The photophysical characterization of **AzoPA** and **dAzoPA** revealed similar properties to classical azobenzenes and other photoswitchable lipids (Figure 2). Both photolipids could be reversibly switched to their respective *cis* and *trans* forms with UV-A (365 nm) and blue light (460 nm) and underwent slow thermal relaxation ($t_{1/2}$ = 678 min in PBS) (Figures 2A–D and S1). Interestingly, the molar absorption of **dAzoPA** at 340 nm is approximately 2 times higher than that of **AzoPA** but almost equally high after switching to the *cis* form, suggesting that both azobenzenes are effectively switched to *cis* upon irradiation. To quantify the absolute amount of the *trans* and *cis* forms of **dAzoPA** after irradiation, we performed NMR studies (Figure 2E). These studies confirmed that both azobenzenes can be effectively switched from their *trans* form (100% total *trans* isomer) to their *cis* form (97% total *cis* isomer) upon irradiation with 365 nm light.

**Cellular Uptake and Metabolism of AzoPA and dAzoPA.** PA has a complex metabolic pathway in mammalian cells (Figure 3A), motivating us to investigate the cellular uptake and metabolism of **AzoPA** and **dAzoPA**. We treated NIH 3T3 mouse embryonic fibroblast cells with these lipids in their *cis* or *trans* forms, precomplexed to fatty-acid-free bovine serum albumin (BSA), for 1 h and then analyzed cellular lipid extracts by HPLC. Because photoswitchable lipids contain a unique azobenzene moiety with a strong absorption at 350 nm in its *trans* form, they are easily distinguishable from endogenous lipids via HPLC. This analysis revealed that *cis* and *trans* forms of both **AzoPA** and **dAzoPA** were taken up to similar extents (Figure 3B,C), corresponding to approximately

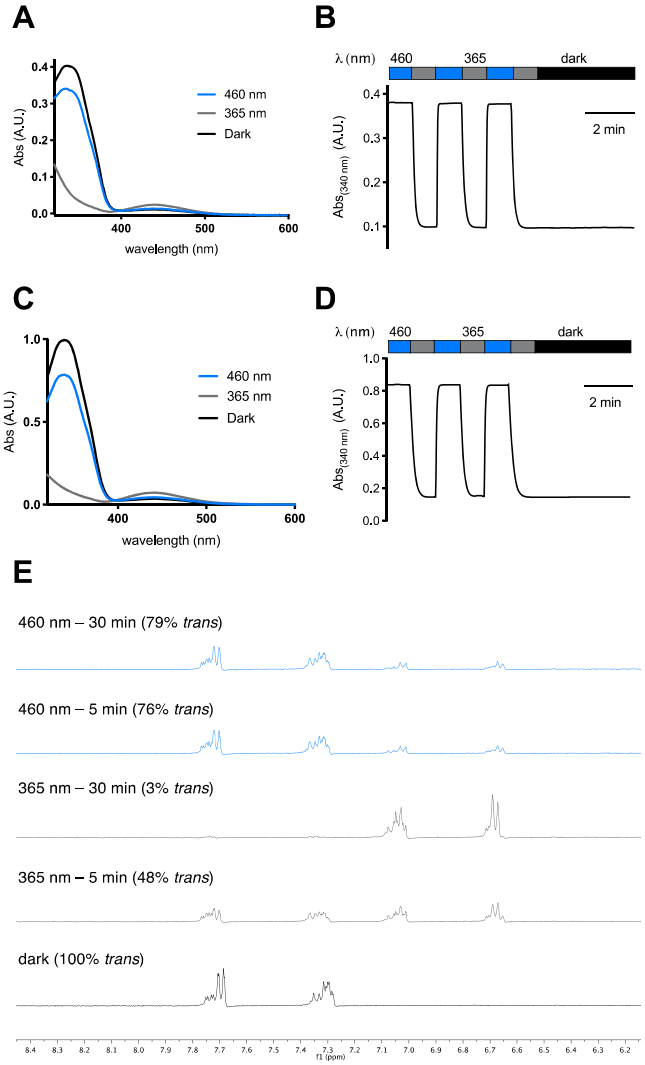


**Figure 2.** Photophysical characterization of **AzoPA** (A,B) and **dAzoPA** (C,D). (A,C) UV–vis spectra of **AzoPA** (A) and **dAzoPA** (C) in the dark-adapted (black, *trans*), 365-nm-adapted (gray, *cis*), and 460-nm-adapted (blue, *trans*) photostationary states (50 $\mu$M, DMSO). (B,D) Reversible cycling between photoisomers with alternating illumination at 365/460 nm for **AzoPA** (B) and **dAzoPA** (D). (E) Nuclear magnetic resonance (NMR) study (performed in DMSO-$d_6$) of the aromatic region of **dAzoPA** before and after irradiation with 365 or 460 nm and quantification of the *trans* form relative to the *cis* form.

$1 \times 10^8$ molecules/cell when cells were treated with 10 $\mu$M photolipid (Figure S2A).

We observed several other azobenzene-containing species that corresponded to photolipid analogues of diacylglycerol (**PhoDAG**), lysophosphatidic acid (**AzoLPA**), fatty acid (**FAAzo4**), and phosphatidylcholine (**AzoPC**), suggesting that **AzoPA** and **dAzoPA** are metabolized similarly to endogenous PA[12] (Figure 3D). The non-PA species were not present in the cell culture media (Figure S2B), suggesting that the conversion occurs inside cells and not in an extracellular environment. Interestingly, these photolipid species, including **AzoPA**, were also observed in cells treated with **AzoLPA** and **PhoDAG** (Figure S2C–E), revealing the interconnectivity of photolipid metabolism. We used deuterium-labeled 16:0(d31)-18:1 PA (d31-POPA) in a pulse-chase experiment to study the rate of turnover in comparison to


https://doi.org/10.1021/acscentsci.1c00444
ACS Cent. Sci. 2021, 7, 1205–1215

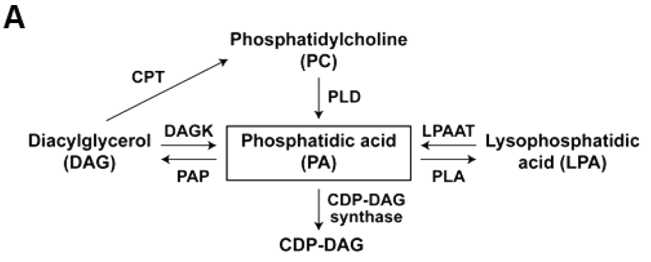


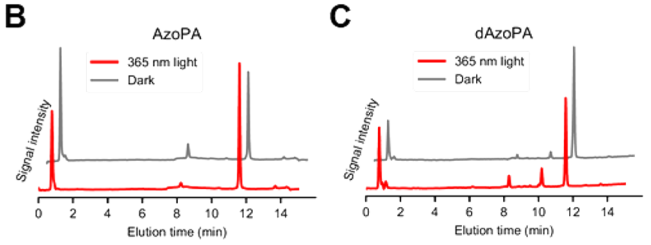


D

| Photoswitchable lipid | Original lipid | Elution time (min) |
|---|---|---|
| PhoDAG | Diacylglycerol | 0.8 |
| FAAzo | Fatty acid | 8.2 |
| AzoPC | Phosphatidylcholine | 10.4 |
| AzoPA | Phosphatidic acid | 11.6 |
| dAzoPA | Phosphatidic acid | 11.6 |
| AzoLPA | Lysophosphatidic acid | 13.9 |

**Figure 3.** Characterization of cellular uptake and metabolism of **AzoPA** and **dAzoPA**. (A) Schematic diagram of mammalian PA metabolism. **CDP**: Cytidine diphosphate, **CPT**: cholinephosphotransferase, **DAGK**: diacylglycerol kinase, **LPAAT**: lysophosphatidic acid acyl transferase, **PAP**: phosphatidic acid phosphatase, **PLA**: phospholipase A, **PLD**: phospholipase D. (B,C) HPLC trace of lipid extracts from NIH 3T3 cells treated with 20 $\mu$M **AzoPA** (B) or **dAzoPA** (C) in the light-induced *cis* form (red) or dark-adapted *trans* form (gray) for 1 h. Just prior to the analysis, all samples were irradiated with 460 nm light to switch azobenzene moieties into the *trans* forms and normalize the absorption. (D) Observed elution times of standard photolipid molecules on HPLC.

**dAzoPA** and found that d31-POPA turnover rates in NIH 3T3 cells were similar to those of the synthetic analogue **dAzoPA** (Figure S2F). Together, our studies validate that both **AzoPA** and **dAzoPA** are effectively incorporated into cells and recognized by endogenous lipid-modifying enzymes.

Our HPLC results show that our PA photolipids can be converted into the corresponding DAG analogues in cells (Figure 2B,C). To evaluate if **AzoPA**/**dAzoPA** metabolism leads to formation of sufficiently large amounts of azobenzene-containing DAG analogues to cause activation of PKC signaling,[29,34] we performed imaging assays using C1-EGFP, a DAG-binding fluorescent probe. Whereas the exogenous addition of a phorbol ester or **PhoDAG** itself led to pronounced translocation of C1-EGFP from the cytosol to the plasma membrane, such translocation was not observed upon addition of **AzoPA** or **dAzoPA** (Figure S2G). These data suggest that the small amounts of **PhoDAG** formed by metabolic conversion of **AzoPA** or **dAzoPA** have negligible effects on PKC signaling.

**Optical Control of mTOR Signaling.** We then studied the bioactivity of **AzoPA** and **dAzoPA** and their abilities to enable control of cellular signaling pathways with light. PA species with unsaturated acyl chains activate the mTOR Complex 1 (mTORC1) through binding to the FKBP12 rapamycin binding (FRB) domain and displacing its inhibitor, DEPTOR.[7] We first tested if the photoswitchable analogues of PA could also affect mTOR signaling and thus manipulate the activity of a key downstream target of mTORC1 signaling, p70-S6 kinase (S6K) (Figure 4A). To examine mTORC1 activation, we measured the levels of S6K phosphorylated at Thr389 (p-S6K) by Western blot analysis. Unlike most other signaling pathways, mTOR signaling has been previously reported to directly respond to 365 nm light.[49] Indeed, we found that intermittent 365 nm light irradiation to cells (5 ms every 15 s) suppressed PA-induced activation of p-S6K (Figure S3A). Thus, to exclude direct effects of light on mTOR signaling, we applied 365 nm light only prior to and not during the incubation with cells to obtain samples with the *cis*-isomer. Serum-starved NIH 3T3 cells were treated with photolipids (**AzoPC**, **AzoPA**, or **dAzoPA**; at 100 $\mu$M, with or without 365 nm light) or natural PA species with different acyl tail compositions of varying degrees of unsaturation (32:0, 34:1, or 36:2) for 1 h. Whereas all the PA species increased p-S6K levels, the unsaturated ones (34:1, 36:2) displayed significantly more activity, in accordance with previous reports (Figure 4B).[7] Both **AzoPA** and **dAzoPA**, but not **AzoPC**, were effective in increasing p-S6K levels, suggesting that the photoswitchable analogues of PA can mimic its bioactivity (Figure 4B).

No differences between the *cis* and *trans* forms were observable at this relatively high concentration (100 $\mu$M); thus, we performed dose−response studies with each isomer to quantify their activities. Excitingly, we found that, of the two pairs of isomeric PA analogues, only a single isomeric compound, *cis*-**dAzoPA**, induced phosphorylation of S6K at lower concentrations (10−20 $\mu$M) (Figure 4C−F). To confirm that this effect was not due to cellular metabolism of **AzoPA** and **dAzoPA**, we analyzed p-S6K level in cells treated with **AzoLPA** or **PhoDAG**, the major metabolites of **AzoPA** and **dAzoPA**. Gratifyingly, we observed no detectable increase in p-S6K levels in these cells, suggesting that **AzoLPA** and **PhoDAG** are not involved in this effect (Figure S3B,C).

To further ascertain the activation of p-S6K, we quantified the amount of phosphorylated ribosomal protein S6 (p-S6), which is a downstream target of p-S6K, by immunofluorescence. Indeed, cells treated with *cis*-**dAzoPA** exhibited a substantial increase in levels of p-S6 (Figure 4G,H), consistent with the previous Western blot analysis of p-S6K levels. Notably, these effects were selective to **dAzoPA** and not **AzoPA**, suggesting a high degree of acyl chain selectivity in PA-induced activation of mTOR signaling. Overall, these studies validate **dAzoPA** as an effective tool for optical control of mTOR signaling via mimicry of PA species with unsaturated acyl tails and underscore the potency of unsaturated forms of PA as effective activators of mTORC1 signaling.

**Optical Control of Hippo Signaling.** Having demonstrated that the photoswitchable PA analogues could activate a well-established PA-dependent pathway, mTOR signaling, with optical control, we next sought to assess the ability of **AzoPA** and **dAzoPA** to modulate Hippo signaling, whose connection to PA signaling was only recently described.[50] The Hippo pathway is an important attenuator of cell growth and proliferation.[10] When Hippo signaling is on, large tumor suppressor 1/2 (LATS1/2) kinases are active and phosphorylate the transcription factor Yes-associated protein (YAP) to prevent its translocation to the nucleus. PA has recently been discovered to modulate Hippo signaling.[8] PA can bind to both LATS1/2 and an upstream factor, NF2, thereby inhibiting Hippo signaling. Using an optogenetic phospholipase D, we


https://doi.org/10.1021/acscentsci.1c00444
ACS Cent. Sci. 2021, 7, 1205−1215

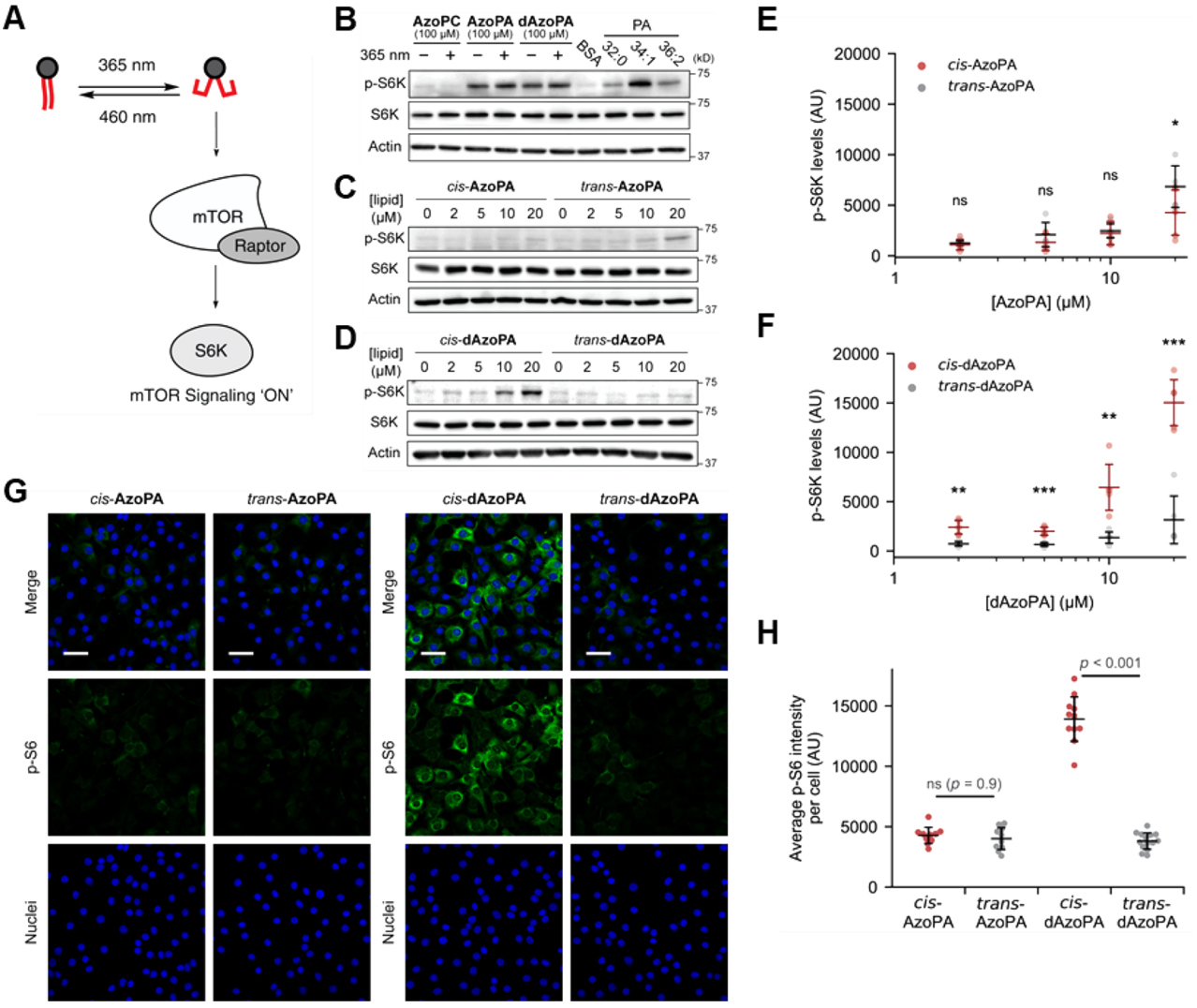


**Figure 4.** Optical control of mTOR signaling in NIH 3T3 cells. (A) Schematic depiction of the optical control of mTOR activation induced by PA. (B) Western blot analysis of NIH 3T3 cells treated with BSA (4 mg/mL) or indicated lipids (100 $\mu$M) for 1 h, probing for p-S6K, S6K, or actin as a loading control. (C,D) Western blot analysis of cells treated with **AzoPA** (C) or **dAzoPA** (D) in their light-induced *cis* form or dark-adapted *trans* form at different concentrations (0−20 $\mu$M) for 30 min. (E,F) Quantification of p-S6K levels in (C) and (D). Horizontal bars indicate mean ($n$ = 6), and vertical error bars indicate standard deviation. Statistical significance was calculated using an unpaired two-tailed Student's $t$ test. *, $p$ < 0.05; **, $p$ < 0.01; ***, $p$ < 0.001. (G) Confocal microscopy images of NIH 3T3 cells treated with the indicated lipids (5 $\mu$M) for 30 min and immunostained for p-S6. Green, p-S6; blue, DAPI (nuclei). Scale bars: 50 $\mu$m. (H) Quantification of immunofluorescence analysis. The plots show average p-S6 intensity per cell in each image. Black horizontal bars indicate mean ($n$ = 10−14), and vertical error bars indicate standard deviation. Statistical significance was calculated using one-way ANOVA, followed by Tukey's HSD test.

have previously demonstrated that the pool of PA that exerts these effects resides at the plasma membrane.[14] In different contexts, PA has been proposed to bind to the Rab-like GTPase RAP2 and thereby modulate Hippo signaling.[51] The full spectrum of PA's roles in affecting Hippo signaling remains to be determined, including the relative importance of different PA species in such regulation. These mechanisms are of vital importance to understand, given the established connection of both PA and the Hippo pathway to the control of cell growth and proliferation in normal physiology and in cancer.[4,5,52]

As a first step toward these goals, we investigated the effects of the photoswitchable PA analogues **AzoPA** and **dAzoPA** on the regulation of Hippo signaling, which can be quantified by measuring nuclear translocation of YAP (Figure 5A). For Hippo signaling, the potency of different PA species has not been reported. We treated serum-starved NIH 3T3 cells with 50 $\mu$M PA with different acyl tail compositions (32:0, 34:1, or 36:2), complexed to bovine serum albumin (BSA), for 1 h and visualized the subcellular location of YAP by immunofluorescence. Interestingly, we found that PA species with unsaturated acyl chains (34:1, 36:2) triggered YAP translocation into nuclei most strongly (Figure 5B,C). However, the fully saturated DPPA was not incorporated as efficiently into lipid−BSA complexes (Figure S4A), which could contribute to the decreased bioactivity observed compared to unsaturated forms of PA. It is worth noting that photoswitchable analogues of PA have similar cellular uptake in their *cis* and *trans* forms (Figure 3B,C), and their ability to be photoswitched *in situ* enables the study of bioactivity of forms with different acyl tail shapes independent from effects on cellular uptake. We thus performed the same experiment using 10 $\mu$M **AzoPA** or **dAzoPA**, with or without preirradiation with 365 nm light to


https://doi.org/10.1021/acscentsci.1c00444
ACS Cent. Sci. 2021, 7, 1205−1215

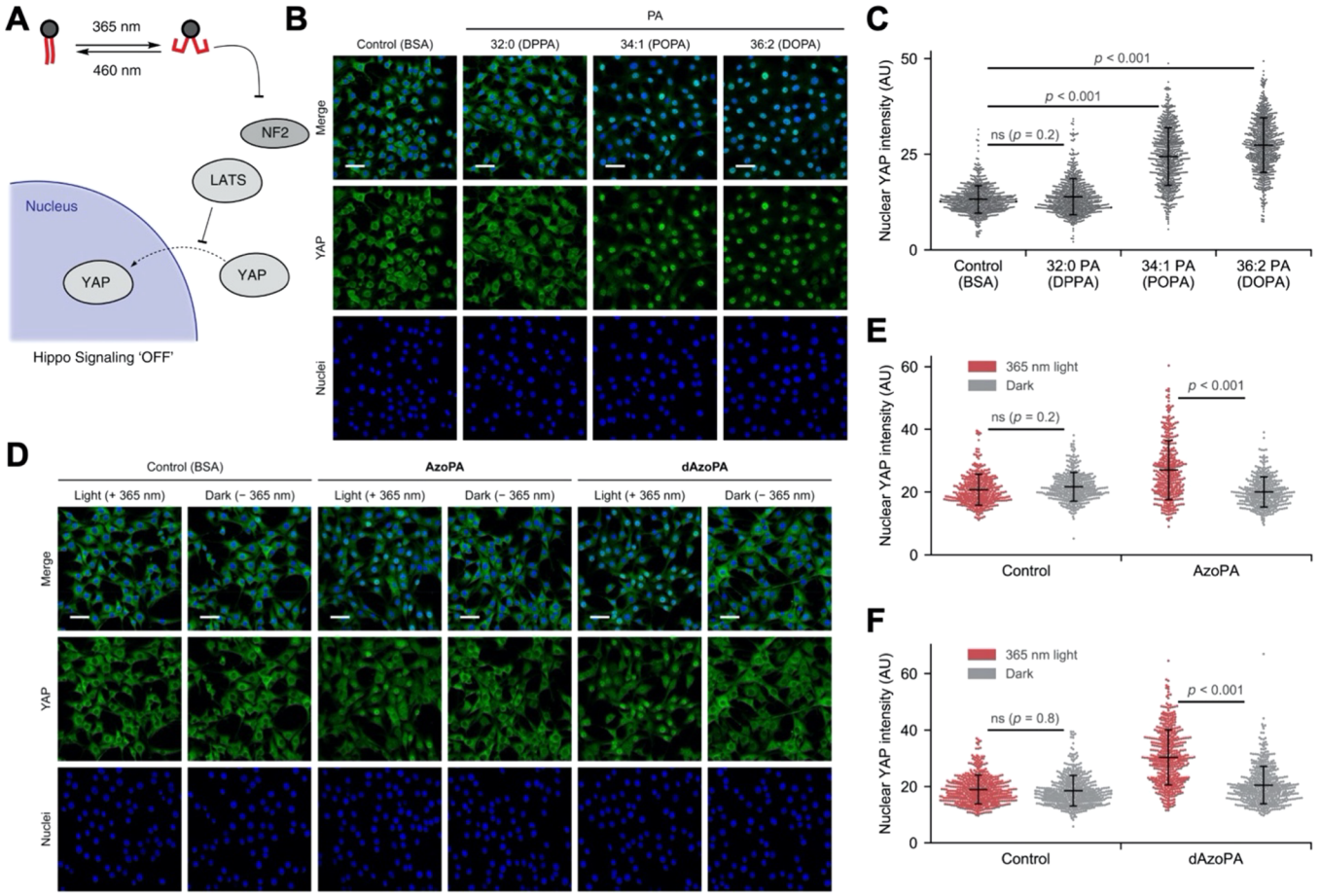


**Figure 5.** Optical control of Hippo signaling in NIH 3T3 cells. (A) Schematic depiction of the optical control of Hippo deactivation induced by PA. (B) Confocal microscopy images of NIH 3T3 cells treated with BSA (4 mg/mL) or the indicated lipids (50 $\mu$M) for 1 h and immunostained for YAP. (C) Quantification of nuclear YAP levels in (B). The plots show mean nuclear YAP intensity in each cell. Black horizontal bars indicate mean ($n$ = 645), and vertical error bars indicate standard deviation. (D) Confocal microscopy images of NIH 3T3 cells treated with BSA (4 mg/mL) or indicated lipids (10 $\mu$M) for 1 h with or without 365 nm light (5 ms every 15 s) and immunostained for YAP. (E,F) Quantification of nuclear YAP levels in (C) and (D). The plots show mean nuclear YAP intensity in each cell. Black horizontal bars indicate mean ($n$ = 342 (C) and 465 (D)), and vertical error bars indicate standard deviation. Statistical significance was calculated using one-way ANOVA, followed by Tukey's HSD test. Green, YAP; blue, DAPI (nuclei). Scale bars: 50 $\mu$m.

obtain their *cis* or *trans* forms. Excitingly, both *cis*-**AzoPA** and *cis*-**dAzoPA**, and not the *trans* isomers, induced nuclear translocation of YAP (Figure 5D−F). Similar results were obtained when 365 nm light was applied after addition of the photolipids to cells in their inactive form to temporally control the photoconversion in cell culture (Figure S4B,C). We also tested two related photoswitchable lipids with different headgroup structures, **AzoPC** and **PhoDAG**. These molecules, in either the *cis* or *trans* forms, did not induce any observable increase in YAP localization (Figure S4D,E), confirming the selectivity of this effect. Collectively, these results suggest that both **AzoPA** and **dAzoPA** can regulate Hippo signaling in a light-dependent manner.

Lysophosphatidic acid (LPA), which is formed from PA by phospholipase A enzymes, can also regulate Hippo signaling via activation of GPCRs from the LPA receptor family.[53] Previous work has established that the effects of PA on Hippo signaling are independent of LPA signaling.[8] Yet, because the photoswitchable PA analogues are distinct molecular species from natural PA, we sought to determine if conversion of **AzoPA** to **AzoLPA**, and subsequent signaling via LPA receptors, was involved in the **AzoPA**-mediated Hippo regulation. For these studies, we used an LPA receptor inhibitor, Ki16425 (LPAi), which blocks the binding of LPA to two major LPA receptors, LPA1 and LPA3, and thus prevents LPA-induced YAP dephosphorylation.[53,54]

We visualized the localization of YAP in cells treated with 10 $\mu$M LPAi for 1 h, followed by treatment with 100 nM **AzoLPA** or 10 $\mu$M **dAzoPA** for 1 h, with or without 365 nm light. Interestingly, *cis*-**AzoLPA**, but not the *trans* form, induced the nuclear translocation of YAP, and this effect was completely blocked by treatment with LPAi (Figure 6A,C). This observation is consistent with the ability of **AzoLPA** to optically control LPA signaling via LPA receptors, as previously assessed by different readouts of LPA receptor activation.[33] By contrast, LPAi had a negligible effect on YAP translocation induced by *cis*-**dAzoPA** (Figure 6B,D). Taken together, these results demonstrate that, although **AzoLPA** can indeed affect Hippo signaling through its binding to the cell surface receptors, it is not involved in the process of Hippo regulation that is mediated by photoswitchable PA analogues.


https://doi.org/10.1021/acscentsci.1c00444
ACS Cent. Sci. 2021, 7, 1205−1215

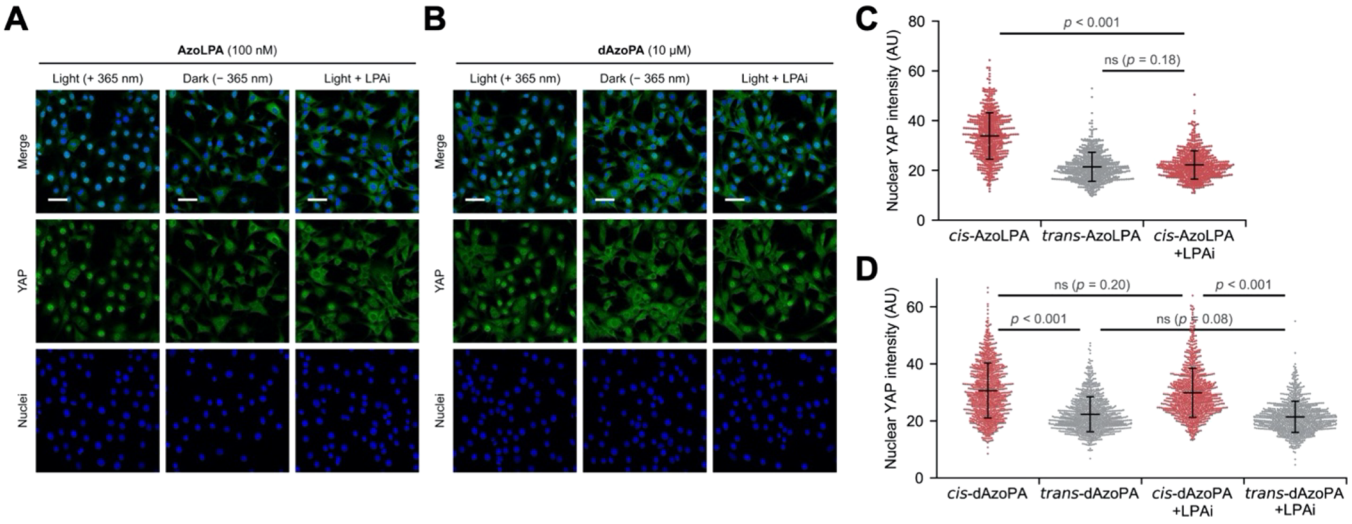


**Figure 6.** Optical control of Hippo signaling in NIH 3T3 cells with the inhibition of LPA receptor signaling. (A,B) Confocal microscopy images of NIH 3T3 cells treated with **AzoLPA** (100 nM) or **dAzoPA** (10 $\mu$M) for 1 h with or without 365 nm light and with or without LPA receptor inhibitor (LPAi: Ki16425, 10 $\mu$M) and immunostained for YAP. Green, YAP; blue, DAPI (nuclei). Scale bars: 50 $\mu$m. (C,D) Quantification of nuclear YAP levels in (A). The plots show mean nuclear YAP intensity in each cell. Black horizontal bars indicate mean ($n$ = 540 (C) and 811 (D)), and vertical error bars indicate standard deviation. Statistical significance was calculated using one-way ANOVA, followed by Tukey's HSD test.

## DISCUSSION

In this study, we developed photoswitchable analogues of PA and demonstrated that they can enable the optical control of two major PA-dependent pathways, mTOR and Hippo signaling. Our photoswitchable analogues, **AzoPA** and **dAzoPA**, were designed to incorporate azobenzene units in their lipid tails, which preserves the integrity of the headgroup and allows these photolipids to effectively mimic the endogenous lipid. Unlike natural PA, however, the photoswitchable PAs allow for optical control of the shape of the acyl tails. We found that the exclusively doubly *cis* form of **dAzoPA** mimics the potent bioactivity of unsaturated species of PA in regulation of mTOR signaling, whereas the *trans* form, and even the *cis* form of **AzoPA**, which still contains a saturated acyl tail at the sn-1 position, have much lower activities, mimicking the relatively inactive, saturated PA species. This finding highlights the remarkable selectivity afforded by **dAzoPA**, which, by virtue of containing two azobenzene photoswitches, undergoes a major light-induced structural rearrangement.

Having validated that photoswitchable PA analogues can effectively modulate an established PA-dependent, oncogenic pathway (mTORC1 signaling), we next investigated the effects of **AzoPA** and **dAzoPA** on Hippo signaling, a recently discovered target of PA. We found that unsaturated forms of PA may be more potent agents at suppressing the Hippo pathway than the saturated forms. Although we cannot decouple the contribution of reduced efficiency of saturated PA (DPPA) in the formation of lipid−BSA complexes, compared to DOPA and POPA, from this effect, both **AzoPA** and **dAzoPA** enabled optical control of this signaling pathway and were more potent in their light-induced *cis* forms. Notably, they can be delivered to cells in one form and subsequently switched, which could potentially allow the study of bioactivity independent of cellular uptake. These results stand in contrast to effects of our photoswitchable PA analogues on mTOR signaling, which is exclusively activated by *cis*-**dAzoPA**. This divergence in activities likely reflects differential lipid-binding requirements of the relevant PA effectors implicated in these two distinct pathways. Nevertheless, our findings highlight an added measure of selectivity afforded by **AzoPA**, in that its photoisomerization can favor activation of one PA-dependent outcome over another. Such unprecedented selectivity suggests the use of the photolipids reported here to decouple the pleiotropy of PA signaling in additional contexts.

Finally, beyond an ability to control PA-dependent signaling pathways, **AzoPA** and **dAzoPA** undergo dynamic metabolism, similar to endogenous PA, as confirmed by HPLC analysis with authentic photolipid standards to detect and assign **AzoPA**- and **dAzoPA**-derived photolipid metabolites in cells. Importantly, using a panel of photolipids and pharmacological manipulations, we ruled out potential effects of the observed photolipid metabolites on mTOR and Hippo signaling in this particular context and ascribe the observed bioactivities to our photoswitchable analogues of PA. Yet, the appearance of azobenzene-derived metabolites of **AzoPA** and **dAzoPA** indicate additional uses of these photolipids as probes of dynamic PA metabolism. Overall, the photolipid analogues of PA presented here comprise a set of tools to control PA signaling and also aid in determining the multiple effects of PA in the context of complex and dynamic lipid metabolic pathways.

## EXPERIMENTAL SECTION

**General Methods.** All reagents and solvents were purchased from commercial sources (Sigma-Aldrich, TCI Europe N.V., Strem Chemicals, etc.) and were used without further purification. Solvents were obtained from Fisher Scientific. Reactions were monitored by thin layer chromatography (TLC) on precoated, Merck Silica gel 60 $F_{254}$ aluminum-backed plates, and the chromatograms were first visualized by UV irradiation at $\lambda$ = 254 nm. Flash silica gel chromatography was performed using silica gel ($SiO_2$, particle size 40−63 $\mu$m) purchased from SiliCycle. NMR spectra were measured on a BRUKER Avance III HD 400 (equipped with a CryoProbe).


https://doi.org/10.1021/acscentsci.1c00444
ACS Cent. Sci. 2021, 7, 1205−1215

Multiplicities in the following experimental procedures are abbreviated as follows: s = singlet, d = doublet, t = triplet, q = quartet, m = multiplet. $^{1}$H chemical shifts are expressed in parts per million (ppm, $\delta$ scale) and are referenced to the residual protium in the NMR solvent ($CDCl_3$: $\delta$ = 7.26; THF-$d_8$: $\delta$ = 1.72). $^{13}$C chemical shifts are expressed in ppm ($\delta$ scale) and are referenced to the carbon resonance of the NMR solvent ($CDCl_3$: $\delta$ = 77.16, THF-$d_8$: $\delta$ = 25.31). NOTE: Due to the *trans*/*cis* isomerization of some compounds containing an azobenzene functionality, more signals were observed in the $^{1}$H and $^{13}$C spectra than would be expected for the pure *trans*-isomer. Only signals for the major *trans*-isomer are reported.

**Synthesis of 1. PhoDAG-1**[34] (50.0 mg, 75.2 mmol, 1.0 equiv) was dissolved in dry $CH_2Cl_2$ (2.0 mL) under a nitrogen atmosphere. Di-*tert*-butyl diisopropylphosphoramidite (37.1 mg, 134 mmol, 1.8 equiv) and 1*H*-tetrazole (0.45 M solution in MeCN, 500 mL) were added, and the solution was stirred for 50 min at room temperature. The mixture was cooled to 0 °C, and *m*CPBA (1.20 g, 7.20 mmol, 3.0 equiv) was added. The mixture was stirred for 30 min at 0 °C and 30 min at room temperature, washed with aqueous $Na_2S_2O_3$ solution (10%) and $NaHCO_3$ solution (saturated), dried, and filtered, and the solvent was evaporated under reduced pressure. The crude mixture was purified by flash column chromatography (4:1 hexanes/ethyl acetate) to yield di-*tert*-butyl AzoPA (**1**) as orange oil (57.2 mg, 66.7 mmol, 89%). $^{1}$H NMR (400 MHz, $CDCl_3$) $\delta$ 7.82 (dd, $J$ = 8.3, 2.9 Hz, 4H), 7.33−7.29 (m, 4H), 5.27−5.21 (m, 1H), 4.38 (dd, $J$ = 12.0, 4.0 Hz, 1H), 4.19−4.05 (m, 3H), 2.71 (dt, $J$ = 18.3, 7.6 Hz, 4H), 2.38 (t, $J$ = 7.4 Hz, 2H), 2.30 (t, $J$ = 7.6 Hz, 2H), 2.04−1.95 (m, 2H), 1.70−1.62 (m, 2H), 1.48−1.46 (m, 18H), 1.42−1.35 (m, 2H), 1.24 (d, $J$ = 4.4 Hz, 30H), 0.94 (t, $J$ = 7.3 Hz, 3H), 0.87 (d, $J$ = 7.0 Hz, 3H). $^{13}$C NMR (100 MHz, $CDCl_3$) $\delta$ 173.5, 172.5, 151.4, 151.1, 146.5, 144.6, 129.3, 129.2, 123.0, 122.9, 82.9, 70.0, 64.5, 62.1, 53.6, 35.7, 35.0, 34.2, 33.6, 33.6, 32.1, 30.0, 30.0, 29.9, 29.8, 29.8, 29.6, 29.5, 29.4, 29.3, 26.4, 25.0, 22.9, 22.5, 14.3, 14.1. $^{31}$P NMR (162 MHz, $CDCl_3$) $\delta$ −9.89. HRMS: $m/z$ calcd. for $C_{49}H_{82}N_2O_8P^+$ ($[M + H]^+$): 857.5803, found: 857.5794.

**Synthesis of AzoPA.** Di-*tert*-butyl AzoPA (**1**) (37.2 mg, 43.4 $\mu$mol, 1.0 equiv) was dissolved in $CH_2Cl_2$ (10 mL). TFA (1.1 mL) was added, and the solution was stirred for 10 min at room temperature. MeOH (128 $\mu$L) was added, and the mixture was stirred for 10 min at room temperature. Toluene (5 mL) was added, and the solvents were removed under reduced pressure. **AzoPA** was obtained as an orange solid (32.2 mg, 43.2 $\mu$mol, quantitative). $^{1}$H NMR (400 MHz, $CDCl_3$) $\delta$ 7.81 (d, $J$ = 8.0 Hz, 4H), 7.29 (d, $J$ = 8.1 Hz, 4H), 5.25 (s, 1H), 4.34 (d, $J$ = 10.2 Hz, 1H), 4.16 (s, 3H), 2.76−2.63 (m, 4H), 2.38 (t, $J$ = 6.9 Hz, 2H), 2.28 (t, $J$ = 7.5 Hz, 2H), 2.03−1.92 (m, 2H), 1.63 (p, $J$ = 7.6 Hz, 2H), 1.55 (s, 2H), 1.37 (q, $J$ = 7.4 Hz, 2H), 1.23 (d, $J$ = 10.1 Hz, 30H), 0.94 (t, $J$ = 7.3 Hz, 3H), 0.87 (t, $J$ = 6.8 Hz, 4H). $^{13}$C NMR (100 MHz, $CDCl_3$) $\delta$ 174.1, 173.2, 151.1, 150.8, 146.7, 144.8, 129.4, 129.2, 123.1, 123.0, 70.0, 65.2, 62.2, 35.7, 34.9, 34.2, 33.6, 33.5, 32.1, 29.9, 29.8, 29.8, 29.7, 29.5, 29.4, 29.3, 26.3, 24.9, 22.8, 22.5, 14.3, 14.1. $^{31}$P NMR (162 MHz, $CDCl_3$) $\delta$ 0.82. HRMS: $m/z$ calcd. for $C_{41}H_{65}N_2O_5^+$ ($[M-PO_3]^+$): 665.4888, found: 665.4897.

**Synthesis of 2.** To a solution of di-*tert*-butyl AzoLPA[33] (20.8 mg, 35.2 $\mu$mol, 1.0 equiv) in dry $CH_2Cl_2$ under nitrogen was added **FAAzo-4**[28] (30.3 mg, 93.3 $\mu$mol, 2.7 equiv), followed by DCC (19.4 mg, 94.0 $\mu$mol, 2.7 equiv) and DMAP (70.0 $\mu$g, 5.60 $\mu$mol, 0.2 equiv). The resulting mixture was stirred for 20 h at room temperature. After this time, the reaction mixture was filtered through a pad of Celite, and the filtrate was concentrated under reduced pressure. The crude product was purified by flash column chromatography (hexane/EtOAc/$Et_3N$, 80:20:0.1 to 70:30:0.1) to yield di-*tert*-butyl dAzoPA (**2**) as an orange oil (24.0 mg, 26.8 $\mu$mol, 76%). $^{1}$H NMR (400 MHz, $CDCl_3$) $\delta$ 7.82 (d, $J$ = 8.0 Hz, 8H), 7.30 (dd, $J$ = 8.1, 4.2 Hz, 8H), 5.28−5.23 (m, 1H), 4.40 (dd, $J$ = 12.0, 4.1 Hz, 1H), 4.19 (dd, $J$ = 12.1, 6.1 Hz,1H), 4.13−4.03 (m, 2H), 2.74−2.63 (m, 7H), 2.40−2.34 (m, 3H), 2.11−1.93 (m, 5H), 1.76−1.62 (m, 6H), 1.46 (s, 18H), 1.42−1.34 (m, 4H), 0.94 (t, $J$ = 7.6 Hz, 6H). $^{13}$C NMR (100 MHz, $CDCl_3$) $\delta$ 172.9, 172.5, 151.4, 151.1, 146.4, 144.5, 144.4, 129.3, 129.2, 129.2, 129.2, 123.0, 122.89, 83.0, 82.9, 82.9, 70.0, 69.9, 64.5, 64.4, 62.3, 49.3, 36.8, 35.7, 35.0, 35.0, 34.1, 33.6, 33.5, 33.4, 33.4, 30.0, 29.9, 29.8, 26.4, 26.3, 25.7, 25.1, 24.8, 22.5, 22.4, 14.1, 14.0. $^{31}$P NMR (162 MHz, $CDCl_3$) $\delta$ −9.92.

**Synthesis of dAzoPA.** Di-*tert*-butyl dAzoPA (**2**) (24.0 mg, 26.8 $\mu$mol, 1.0 equiv) was dissolved in $CH_2Cl_2$ (5.2 mL). TFA (1.3 mL) was added, and the solution was stirred for 10 min at room temperature. MeOH (75 $\mu$L) was added, and the mixture was stirred for 10 min at room temperature. Toluene (15 mL) was added, and the solvents were removed under reduced pressure. **dAzoPA** was obtained as an orange solid (20.8 mg, 26.5 $\mu$mol, quantitative). $^{1}$H NMR (400 MHz, THF-$d_8$) $\delta$ 7.80 (d, $J$ = 6.2 Hz, 8H), 7.31 (d, $J$ = 7.9 Hz, 8H), 5.26 (br. s, 1H), 4.40 (dd, $J$ = 11.8, 3.6 Hz, 1H), 4.20 (dd, $J$ = 12.4, 6.3 Hz,1H), 4.16−4.08 (m, 2H), 2.75−2.65 (m, 7H), 2.41−2.31 (m, 3H), 2.01−1.92 (m, 3H), 1.69−1.61 (m, 5H), 1.44−1.34 (m, 4H), 0.94 (t, $J$ = 7.4 Hz, 6H). $^{13}$C NMR (100 MHz, THF-$d_8$) $\delta$ 173.2, 173.0, 152.3, 152.1, 147.2, 146.3, 146.2, 130.2, 130.1, 130.1, 130.0, 123.8, 123.7, 123.7, 63.1, 55.1, 49.3, 36.4, 35.8, 35.8, 34.9, 34.6, 33.9, 27.5, 27.4, 26.0, 23.4, 14.4. $^{31}$P NMR (162 MHz, THF-$d_8$) $\delta$ 1.07. HRMS: $m/z$ calcd. for $C_{43}H_{53}N_4O_5$ ($[M-PO_3]^+$): 705.4010, found: 705.3994.

**Photophysical Characterization.** UV−vis spectra were recorded using a Varian Cary 50 Bio UV−visible Spectrophotometer. Photoswitching was achieved using 365 or 460 nm LED light sources. The LEDs were pointed directly onto the top of the sample cuvette with **AzoPA** (50 $\mu$M in DMSO). An initial spectrum was recorded (dark-adapted state) and then again following illumination at 365 nm for 30 s (*cis*-adapted state). A third spectrum was recorded after irradiation at 460 nm for 30 s (*trans*-adapted state). Absorption at 340 nm was recorded over several switching cycles while alternating illumination at 365 and 460 nm with. The light source was directly pointed onto the top of the sample cuvette.

**Mammalian Cell Culture.** NIH 3T3 mouse fibroblast cells were grown in DMEM (Corning) supplemented with 10% bovine calf serum (Corning) and 1% penicillin/streptomycin (Corning) at 37 °C in a 5% $CO_2$ atmosphere. For serum starvation, NIH 3T3 cells were cultured in DMEM supplemented with 1% penicillin/streptomycin (serum-free medium). For experiments, cells were seeded in 12-well plates for Western blot analysis, 35 mm glass-bottom imaging dishes (MatTek Corporation) for immunofluorescence, and 35 mm dishes for HPLC and LC−MS analysis. For C1-EGFP translocation assays, cells seeded on 35 mm imaging dishes were transfected using 1 $\mu$g of C1-EGFP plasmid (a gift from the De Camilli laboratory, Yale University, New Haven, CT) and 3 $\mu$L of Lipofectamine 2000 (Invitrogen) per dish, 24 h prior to the experiment.


https://doi.org/10.1021/acscentsci.1c00444
ACS Cent. Sci. 2021, 7, 1205−1215

**Preparation of Lipid−BSA Complexes.** Photoswitchable lipid analogues were synthesized in the lab, and PA was purchased (DPPA, Cayman, 15082; POPA, Avanti Polar Lipids, 840857; DOPA, Avanti Polar Lipids, 840875). The lipid was dissolved in chloroform and dried under a stream of $N_2$ gas to form a lipid film. The lipid film was resuspended, with sonication, in 4 mg/mL of fatty-acid-free BSA (Sigma-Aldrich, A8806) in DPBS (Corning) to a final concentration of 1 mM lipid to generate a stock solution. For **PhoDAG**, because of its low solubility in aqueous solution,[30] the lipid film was resuspended in DMSO to a final concentration of 10 mM. For isomerization to the *cis* form, the lipid solution was treated with 365 nm light for 10 min using a UV lamp (Thermo Fisher, # UVP95004207) prior to addition to cells.

**HPLC and LC−MS Analysis of Lipid Extracts.** NIH 3T3 cells were starved in serum-free medium for 20 h, and cells were treated with the indicated lipids (5−20 $\mu$M lipid in the form of lipid−BSA complexes, with or without pretreatment of 5 min illumination with 365 nm light) for 30 min or 1 h. After the incubation, cells were rinsed with PBS for three times, and lipid extracts were obtained using a modified Bligh−Dyer extraction as reported previously.[14] Briefly, cells were scraped in 250 $\mu$L of methanol, 125 $\mu$L of acetic acid (20 mM in water), and 100 $\mu$L of PBS using cell scrapers (Corning), and the suspension was transferred into 1.5 mL microcentrifuge tubes. After the addition of 500 $\mu$L of chloroform, the mixture was vortexed vigorously for 5 min and centrifuged at 17 000*g* for 1 min. The organic layer (bottom) was collected in a new tube and dried under a stream of $N_2$ gas to obtain a lipid film, which was then resuspended in chloroform. For HPLC analysis, the lipid solution was irradiated with blue light (488 nm laser) for 10 s and quickly injected into a Shimadzu Prominence HPLC equipped with an in-line fluorescence detector. Separation was achieved using a Luna 3 $\mu$m Silica LC Column (Phenomenex; 150 × 4.6 mm) with a binary gradient elution system where solvent A was chloroform/methanol/ammonium hydroxide (95:7:0.5), and solvent B was chloroform/methanol/water/ammonium hydroxide (60:34:5:0.5). For LC−MS analysis, the lipid solution was analyzed on an Agilent 6230 electrospray ionization−time-of-flight MS coupled to an Agilent 1260 HPLC equipped with a Luna 3 $\mu$m Silica LC Column (Phenomenex; 50 × 2 mm) using a binary gradient elution system where solvent A was chloroform/methanol/ammonium hydroxide (85:15:0.5), and solvent B was chloroform/methanol/water/ammonium hydroxide (60:34:5:0.5).

**Quantification of Lipids in Lipid−BSA Complexes.** Lipid−BSA complexes were separated from free lipids by size-exclusion chromatography using an ÄKTA pure system equipped with a Superdex 200 Increase 10/300 GL column in PBS. The fractions containing BSA were subjected to Bligh−Dyer lipid extraction as described above, and the obtained lipid extracts were analyzed by LC−MS as described above.

**Evaluation of mTORC1 Activity.** NIH 3T3 cells were starved in serum-free medium for 20 h, and cells were treated with the indicated lipids (10 $\mu$M lipid in the form of lipid−BSA complexes with or without pretreatment of 5 min illumination with 365 nm light) for 30 min or 1 h. For Western blot analysis, cells were lysed in RIPA lysis buffer (50 mM Tris-HCl, pH 7.4, 150 mM NaCl, 1% Triton-X, 0.5% sodium deoxycholate, 0.1% SDS, 1 mM EDTA, 1× cOmplete Protease Inhibitor, 1 mM sodium orthovanadate). The membrane was blotted with antibodies for phospho-p70 S6 kinase (Thr389) (Cell Signaling Technology, #9205), p70 S6 kinase (Santa Cruz Biotechnology, sc-8418), or actin (MP Biomedicals, 08691001), with detection by chemiluminescence using the Clarity Western ECL Substrate (Bio-Rad) and acquisition on a Bio-Rad ChemiDoc MP System. For immunofluorescence, sample preparation and confocal microscopy were performed as reported previously.[14] Briefly, cells were fixed with 4% formaldehyde for 10 min, permeabilized with 0.5% Triton X-100 in PBS for 5 min, and blocked with 1% BSA and 0.1% Tween-20 in PBS (blocking buffer) for 30 min. Primary antibody incubation was performed with a 1:250 dilution of a phospho-S6 (Ser240/244) antibody (Cell Signaling Technology, #5364), and secondary antibody incubation was performed with a 1:500 dilution of antimouse−Alexa Fluor 488 (Invitrogen, A-21202). Image acquisition by laser-scanning confocal microscopy was performed as described before by using solid-state lasers (405, 488 nm) to excite DAPI and Alexa Fluor 488, respectively.[14] For calculation of the average p-S6 intensity per cell, the total integrated density of p-S6 signal in the frame was measured and divided by the number of cells in the frame using FIJI and a Python script: "Intensity_per_cell.py".

**Evaluation of Nuclear YAP Localization.** NIH 3T3 cells were starved in serum-free medium for 6 h, and cells were treated with the indicated lipids (10 $\mu$M lipid in the form of a lipid−BSA complex, with or without pretreatment of 5 min illumination with 365 nm light) for 1 h with or without 365 nm light (5 ms of illumination at 15 s intervals). For experiments with LPA receptor inhibitor, cells were pretreated with 10 $\mu$M Ki16425 (Cayman Chemical Company, 10012659) for 1 h. Immunofluorescence analysis was performed as described above, and primary antibody incubation was done with 1:200 dilution of YAP antibody (Santa Cruz Biotechnology, sc-101199). For statistical analysis of YAP nuclear intensity, the mean of YAP signal in each nucleus was collected using FIJI and a Python script: "Nuclear_intensity.py".

**Safety Statement.** No unexpected or unusually high safety hazards were encountered.

## ■ ASSOCIATED CONTENT

### Supporting Information

The Supporting Information is available free of charge at https://pubs.acs.org/doi/10.1021/acscentsci.1c00444.

$^1$H and $^{13}$C NMR spectra, Python scripts, and Supplementary Figures (PDF)

## ■ AUTHOR INFORMATION


### Corresponding Authors

**Dirk Trauner** − *Department of Chemistry, New York University, New York, New York 10003, United States;* orcid.org/0000-0002-6782-6056; Email: dirktrauner@nyu.edu

**Jeremy M. Baskin** − *Department of Chemistry and Chemical Biology and Weill Institute for Cell and Molecular Biology, Cornell University, Ithaca, New York 14850, United States;* orcid.org/0000-0003-2939-3138; Email: jeremy.baskin@cornell.edu

### Authors

**Reika Tei** − *Department of Chemistry and Chemical Biology and Weill Institute for Cell and Molecular Biology, Cornell University, Ithaca, New York 14850, United States*

**Johannes Morstein** − *Department of Chemistry, New York University, New York, New York 10003, United States;* orcid.org/0000-0002-6940-288X

**Andrej Shemet** − *Department of Chemistry, New York University, New York, New York 10003, United States*

Complete contact information is available at: https://pubs.acs.org/10.1021/acscentsci.1c00444


### Author Contributions

#R.T. and J.M. contributed equally to this work.

### Notes

The authors declare no competing financial interest.

## ■ ACKNOWLEDGMENTS

J.M.B. acknowledges support from a Beckman Young Investigator award, a Sloan Research Fellowship, and the NSF (CAREER CHE-1749919). D.T. acknowledges support from NYU. R.T. was supported by Honjo International, Funai Overseas, and Cornell Fellowships. J.M. thanks the German Academic Scholarship Foundation for a fellowship, the New York University for a MacCracken fellowship and a Margaret and Herman Sokol fellowship, and the NCI for an F99/K00 award (1F99CA253758-01). We thank the Fromme lab for use of equipment.

## ■ REFERENCES


(1) Liu, Y.; Su, Y.; Wang, X. Phosphatidic Acid-Mediated Signaling. *Lipid-mediated Protein Signaling* **2013**, *991*, 159−176.

(2) Kooijman, E. E.; Burger, K. N. J. Biophysics and Function of Phosphatidic Acid: A Molecular Perspective. *Biochim. Biophys. Acta, Mol. Cell Biol. Lipids* **2009**, *1791* (9), 881−888.

(3) Tanguy, E.; Wang, Q.; Moine, H.; Vitale, N. Phosphatidic Acid: From Pleiotropic Functions to Neuronal Pathology. *Front. Cell. Neurosci.* **2019**, *13*, 2.

(4) Gomez-Cambronero, J. Phosphatidic Acid, Phospholipase D and Tumorigenesis. *Adv. Biol. Regul.* **2014**, *54*, 197−206.

(5) Bruntz, R. C.; Lindsley, C. W.; Brown, H. A. Phospholipase D Signaling Pathways and Phosphatidic Acid as Therapeutic Targets in Cancer. *Pharmacol. Rev.* **2014**, *66* (4), 1033−1079.

(6) Fang, Y.; Vilella-Bach, M.; Bachmann, R.; Flanigan, A.; Chen, J. Phosphatidic Acid-Mediated Mitogenic Activation of MTOR Signaling. *Science* **2001**, *294* (5548), 1942−1945.

(7) Yoon, M.-S.; Rosenberger, C. L.; Wu, C.; Truong, N.; Sweedler, J. V.; Chen, J. Rapid Mitogenic Regulation of the MTORC1 Inhibitor, DEPTOR, by Phosphatidic Acid. *Mol. Cell* **2015**, *58* (3), 549−556.

(8) Han, H.; Qi, R.; Zhou, J. J.; Ta, A. P.; Yang, B.; Nakaoka, H. J.; Seo, G.; Guan, K.-L.; Luo, R.; Wang, W. Regulation of the Hippo Pathway by Phosphatidic Acid-Mediated Lipid-Protein Interaction. *Mol. Cell* **2018**, *72* (2), 328−340.e8.

(9) Saxton, R. A.; Sabatini, D. M. MTOR Signaling in Growth, Metabolism, and Disease. *Cell* **2017**, *168* (6), 960−976.

(10) Yu, F.-X.; Zhao, B.; Guan, K.-L. Hippo Pathway in Organ Size Control, Tissue Homeostasis, and Cancer. *Cell* **2015**, *163* (4), 811−828.

(11) Winter, J. N.; Fox, T. E.; Kester, M.; Jefferson, L. S.; Kimball, S. R. Phosphatidic Acid Mediates Activation of MTORC1 through the ERK Signaling Pathway. *Am. J. Physiol.-Cell Physiol.* **2010**, *299* (2), C335−C344.

(12) Bond, P. Phosphatidic Acid: Biosynthesis, Pharmacokinetics, Mechanisms of Action and Effect on Strength and Body Composition in Resistance-Trained Individuals. *Nutr. Metab.* **2017**, *14* (1), 12.

(13) Athenstaedt, K.; Daum, G. Phosphatidic Acid, a Key Intermediate in Lipid Metabolism. *Eur. J. Biochem.* **1999**, *266* (1), 1−16.

(14) Tei, R.; Baskin, J. M. Spatiotemporal Control of Phosphatidic Acid Signaling with Optogenetic, Engineered Phospholipase Ds. *J. Cell Biol.* **2020**, *219*, No. e201907013.

(15) Beharry, A. A.; Woolley, G. A. Azobenzene Photoswitches for Biomolecules. *Chem. Soc. Rev.* **2011**, *40* (8), 4422−4437.

(16) Lerch, M. M.; Hansen, M. J.; van Dam, G. M.; Szymanski, W.; Feringa, B. L. Emerging Targets in Photopharmacology. *Angew. Chem., Int. Ed.* **2016**, *55* (37), 10978−10999.

(17) Hüll, K.; Morstein, J.; Trauner, D. In Vivo Photopharmacology. *Chem. Rev.* **2018**, *118* (21), 10710−10747.

(18) Höglinger, D.; Nadler, A.; Schultz, C. Caged Lipids as Tools for Investigating Cellular Signaling. *Biochim. Biophys. Acta, Mol. Cell Biol. Lipids* **2014**, *1841* (8), 1085−1096.

(19) Dinkel, C.; Wichmann, O.; Schultz, C. Versatile Reagents to Introduce Caged Phosphates. *Tetrahedron Lett.* **2003**, *44* (6), 1153−1155.

(20) Wagner, N.; Schuhmacher, M.; Lohmann, A.; Nadler, A. A Coumarin Triflate Reagent Enables One-Step Synthesis of Photo-Caged Lipid Metabolites for Studying Cell Signaling. *Chem. - Eur. J.* **2019**, *25* (68), 15483−15487.

(21) Williger, B.-T.; Reich, R.; Neeman, M.; Bercovici, T.; Liscovitch, M. Release of Gelatinase A (Matrix Metalloproteinase 2) Induced by Photolysis of Caged Phosphatidic Acid in HT 1080 Metastatic Fibrosarcoma Cells. *J. Biol. Chem.* **1995**, *270* (50), 29656−29659.

(22) Goedhart, J.; Gadella, T. W. J. Photolysis of Caged Phosphatidic Acid Induces Flagellar Excision in Chlamydomonas. *Biochemistry* **2004**, *43* (14), 4263−4271.

(23) Nadler, A.; Yushchenko, D. A.; Müller, R.; Stein, F.; Feng, S.; Mulle, C.; Carta, M.; Schultz, C. Exclusive Photorelease of Signalling Lipids at the Plasma Membrane. *Nat. Commun.* **2015**, *6*, 10056.

(24) Wagner, N.; Stephan, M.; Höglinger, D.; Nadler, A. A Click Cage: Organelle-Specific Uncaging of Lipid Messengers. *Angew. Chem., Int. Ed.* **2018**, *57* (40), 13339−13343.

(25) Feng, S.; Harayama, T.; Montessuit, S.; David, F. P.; Winssinger, N.; Martinou, J.-C.; Riezman, H. Mitochondria-Specific Photoactivation to Monitor Local Sphingosine Metabolism and Function. *eLife* **2018**, *7*, No. e34555.

(26) Feng, S.; Harayama, T.; Chang, D.; Hannich, J. T.; Winssinger, N.; Riezman, H. Lysosome Targeted Photoactivation Reveals Local Sphingosine Metabolism Signature. *Chem. Sci.* **2019**, *10*, 2253.

(27) Morstein, J.; Impastato, A. C.; Trauner, D. Photoswitchable Lipids. *ChemBioChem* **2021**, *22*, 73.

(28) Frank, J. A.; Moroni, M.; Moshourab, R.; Sumser, M.; Lewin, G. R.; Trauner, D. Photoswitchable Fatty Acids Enable Optical Control of TRPV1. *Nat. Commun.* **2015**, *6*, 7118.

(29) Lichtenegger, M.; Tiapko, O.; Svobodova, B.; Stockner, T.; Glasnov, T. N.; Schreibmayer, W.; Platzer, D.; de la Cruz, G. G.; Krenn, S.; Schober, R.; Shrestha, N.; Schindl, R.; Romanin, C.; Groschner, K. An Optically Controlled Probe Identifies Lipid-Gating Fenestrations within the TRPC3 Channel. *Nat. Chem. Biol.* **2018**, *14* (4), 396−404.

(30) Leinders-Zufall, T.; Storch, U.; Bleymehl, K.; Mederos y Schnitzler, M.; Frank, J. A.; Konrad, D. B.; Trauner, D.; Gudermann, T.; Zufall, F. PhoDAGs Enable Optical Control of Diacylglycerol-Sensitive Transient Receptor Potential Channels. *Cell Chem. Biol.* **2018**, *25* (2), 215−223.e3.

(31) Frank, J. A.; Yushchenko, D.; Fine, N. H. F.; Duca, M.; Citir, M.; Broichhagen, J.; Hodson, D. J.; Schultz, C.; Trauner, D. Optical Control of GPR40 Signalling in Pancreatic β-Cells. *Chem. Sci.* **2017**, *8*, 7604.

(32) Morstein, J.; Hill, R. Z.; Novak, A. J. E.; Feng, S.; Norman, D. D.; Donthamsetti, P. C.; Frank, J. A.; Harayama, T.; Williams, B. M.; Parrill, A. L.; Tigyi, G. J.; Riezman, H.; Isacoff, E. Y.; Bautista, D. M.; Trauner, D. Optical Control of Sphingosine-1-Phosphate Formation and Function. *Nat. Chem. Biol.* **2019**, *15* (6), 623.

(33) Morstein, J.; Dacheux, M. A.; Norman, D. D.; Shemet, A.; Donthamsetti, P. C.; Citir, M.; Frank, J. A.; Schultz, C.; Isacoff, E. Y.; Parrill, A. L.; Tigyi, G. J.; Trauner, D. Optical Control of Lysophosphatidic Acid Signaling. *J. Am. Chem. Soc.* **2020**, *142*, 10612.
(34) Frank, J. A.; Yushchenko, D. A.; Hodson, D. J.; Lipstein, N.; Nagpal, J.; Rutter, G. A.; Rhee, J.-S.; Gottschalk, A.; Brose, N.; Schultz, C.; Trauner, D. Photoswitchable Diacylglycerols Enable Optical Control of Protein Kinase C. *Nat. Chem. Biol.* **2016**, *12* (9), 755−762.
(35) Kol, M.; Williams, B.; Toombs-Ruane, H.; Franquelim, H. G.; Korneev, S.; Schroeer, C.; Schwille, P.; Trauner, D.; Holthuis, J. C.; Frank, J. A. Optical Manipulation of Sphingolipid Biosynthesis Using Photoswitchable Ceramides. *eLife* **2019**, *8*, No. e43230.
(36) Morstein, J.; Awale, M.; Reymond, J.-L.; Trauner, D. Mapping the Azolog Space Enables the Optical Control of New Biological Targets. *ACS Cent. Sci.* **2019**, *5* (4), 607−618.
(37) Morstein, J.; Trads, J. B.; Hinnah, K.; Willems, S.; Barber, D. M.; Trauner, M.; Merk, D.; Trauner, D. Optical Control of the Nuclear Bile Acid Receptor FXR with a Photohormone. *Chem. Sci.* **2020**, *11* (2), 429−434.
(38) Hinnah, K.; Willems, S.; Morstein, J.; Heering, J.; Hartrampf, F. W. W.; Broichhagen, J.; Leippe, P.; Merk, D.; Trauner, D. Photohormones Enable Optical Control of the Peroxisome Proliferator-Activated Receptor γ (PPARγ). *J. Med. Chem.* **2020**, *63* (19), 10908−10920.
(39) Hartrampf, N.; Seki, T.; Baumann, A.; Watson, P.; Vepřek, N. A.; Hetzler, B. E.; Hoffmann-Röder, A.; Tsuji, M.; Trauner, D. Optical Control of Cytokine Production Using Photoswitchable Galactosyl-ceramides. *Chem. - Eur. J.* **2020**, *26* (20), 4476−4479.
(40) Hu, H.-G.; Chen, P.-G.; Wang, G.; Wu, J.-J.; Zhang, B.-D.; Li, W.-H.; Davis, R. L.; Li, Y.-M. Regulation of Immune Activation by Optical Control of TLR1/2 Heterodimerization. *ChemBioChem* **2020**, *21* (8), 1150.
(41) Anzai, J.-I.; Osa, T. Photosensitive Artificial Membranes Based on Azobenzene and Spirobenzopyran Derivatives. *Tetrahedron* **1994**, *50* (14), 4039−4070.
(42) Kinoshita, T. Photoresponsive Membrane Systems. *J. Photochem. Photobiol., B* **1998**, *42* (1), 12−19.
(43) Frank, J. A.; Franquelim, H. G.; Schwille, P.; Trauner, D. Optical Control of Lipid Rafts with Photoswitchable Ceramides. *J. Am. Chem. Soc.* **2016**, *138* (39), 12981−12986.
(44) Pernpeintner, C.; Frank, J. A.; Urban, P.; Roeske, C. R.; Pritzl, S. D.; Trauner, D.; Lohmüller, T. Light-Controlled Membrane Mechanics and Shape Transitions of Photoswitchable Lipid Vesicles. *Langmuir* **2017**, *33* (16), 4083−4089.
(45) Urban, P.; Pritzl, S. D.; Konrad, D. B.; Frank, J. A.; Pernpeintner, C.; Roeske, C. R.; Trauner, D.; Lohmüller, T. Light-Controlled Lipid Interaction and Membrane Organization in Photolipid Bilayer Vesicles. *Langmuir* **2018**, *34* (44), 13368−13374.
(46) Urban, P.; Pritzl, S. D.; Ober, M. F.; Dirscherl, C. F.; Pernpeintner, C.; Konrad, D. B.; Frank, J. A.; Trauner, D.; Nickel, B.; Lohmueller, T. A Lipid Photoswitch Controls Fluidity in Supported Bilayer Membranes. *Langmuir* **2020**, *36* (10), 2629−2634.
(47) Foster, D. A. Phosphatidic Acid and Lipid-Sensing by MTOR. *Trends Endocrinol. Metab.* **2013**, *24* (6), 272−278.
(48) Zhang, C.; Wendel, A. A.; Keogh, M. R.; Harris, T. E.; Chen, J.; Coleman, R. A. Glycerolipid Signals Alter MTOR Complex 2 (MTORC2) to Diminish Insulin Signaling. *Proc. Natl. Acad. Sci. U. S. A.* **2012**, *109* (5), 1667−1672.
(49) Strozyk, E.; Kulms, D. The Role of AKT/MTOR Pathway in Stress Response to UV-Irradiation: Implication in Skin Carcinogenesis by Regulation of Apoptosis, Autophagy and Senescence. *Int. J. Mol. Sci.* **2013**, *14* (8), 15260−15285.
(50) Totaro, A.; Piccolo, S. Phosphatidic Acid Enters into the YAP/TAZ Arena. *Trends Mol. Med.* **2019**, *25* (1), 5−7.
(51) Meng, Z.; Qiu, Y.; Lin, K. C.; Kumar, A.; Placone, J. K.; Fang, C.; Wang, K.-C.; Lu, S.; Pan, M.; Hong, A. W.; Moroishi, T.; Luo, M.; Plouffe, S. W.; Diao, Y.; Ye, Z.; Park, H. W.; Wang, X.; Yu, F.-X.; Chien, S.; Wang, C.-Y.; Ren, B.; Engler, A. J.; Guan, K.-L. RAP2Mediates Mechanoresponses of the Hippo Pathway. *Nature* **2018**, *560* (7720), 655−660.
(52) Lin, K. C.; Park, H. W.; Guan, K.-L. Deregulation and Therapeutic Potential of the Hippo Pathway in Cancer. *Annu. Rev. Cancer Biol.* **2018**, *2* (1), 59−79.
(53) Yu, F.-X.; Zhao, B.; Panupinthu, N.; Jewell, J. L.; Lian, I.; Wang, L. H.; Zhao, J.; Yuan, H.; Tumaneng, K.; Li, H.; Fu, X.-D.; Mills, G. B.; Guan, K.-L. Regulation of the Hippo-YAP Pathway by G-Protein-Coupled Receptor Signaling. *Cell* **2012**, *150* (4), 780−791.
(54) Ohta, H.; Sato, K.; Murata, N.; Damirin, A.; Malchinkhuu, E.; Kon, J.; Kimura, T.; Tobo, M.; Yamazaki, Y.; Watanabe, T.; Yagi, M.; Sato, M.; Suzuki, R.; Murooka, H.; Sakai, T.; Nishitoba, T.; Im, D.-S.; Nochi, H.; Tamoto, K.; Tomura, H.; Okajima, F. Ki16425, a Subtype-Selective Antagonist for EDG-Family Lysophosphatidic Acid Receptors. *Mol. Pharmacol.* **2003**, *64* (4), 994−1005.


https://doi.org/10.1021/acscentsci.1c00444
*ACS Cent. Sci.* 2021, 7, 1205−1215